ORIGINAL PAPER

Physiology-based modeling of cortical auditory evoked potentials

C. C. Kerr · C. J. Rennie · P. A. Robinson

Abstract Evoked potentials are the transient electrical responses caused by changes in the brain following stimuli. This work uses a physiology-based continuum model of neuronal activity in the human brain to calculate theoretical cortical auditory evoked potentials (CAEPs) from the model's linearized response. These are fitted to experimental data, allowing the fitted parameters to be related to brain physiology. This approach yields excellent fits to CAEP data, which can then be compared to fits of EEG spectra. It is shown that the differences between resting eyes-open EEG and standard CAEPs can be explained by changes in the physiology of populations of neurons in corticothalamic pathways, with notable similarities to certain aspects of slow-wave sleep. This pilot study demonstrates the ability of our model-based fitting method to provide information on the underlying physiology of the brain that is not available using standard methods.

C. C. Kerr (✉) · C. J. Rennie · P. A. Robinson
School of Physics, University of Sydney,
Sydney, NSW 2006, Australia
e-mail: ckerr@physics.usyd.edu.au

C. C. Kerr · C. J. Rennie · P. A. Robinson
Brain Dynamics Center,
Westmead Hospital, Westmead, NSW 2145, Australia

C. J. Rennie
Department of Medical Physics, Westmead Hospital,
Westmead, NSW 2145, Australia
e-mail: rennie@physics.usyd.edu.au

P. A. Robinson
Faculty of Medicine, University of Sydney,
Sydney, NSW 2006, Australia
e-mail: robinson@physics.usyd.edu.au

1 Introduction

Evoked potentials (EPs) are the components of the electroencephalogram (EEG) that occur in response to brief stimuli, including tones, flashes, and electric shocks. The brain's electrical responses to these stimuli are superposed with ongoing EEG activity, and to improve the signal to noise ratio, EPs are typically obtained by averaging over several hundred stimuli (Picton et al. 2000), since the EP is time-locked to the stimulus while other EEG activity is not. It is not known whether EPs are generated by the activation of additional networks, or by changes in networks already active during resting EEG; it is possible that early features of the response are due to the former, while later features are due to the latter (Näätänen and Picton 1987).

In the auditory oddball paradigm, used here, frequent low-pitched "standard" tones are interspersed pseudorandomly with rarer high-pitched "target" tones, to which the subject responds. This paper will focus on CAEPs resulting from standard tones, where no response is required, since target CAEPs require a greater degree of cognition, and hence present additional complexities. A typical standard CAEP is shown in Fig. 1.

Physiological changes underlie the observed electrical response, and hence EPs contain information about how the brain carries out stimulus processing (Kotchoubey 2005). It has been shown that CAEPs display systematic changes in amplitude and latency depending on the stimulus characteristics, task instructions, and age, and on conditions such as depression and schizophrenia (Picton et al. 2000). Hence,
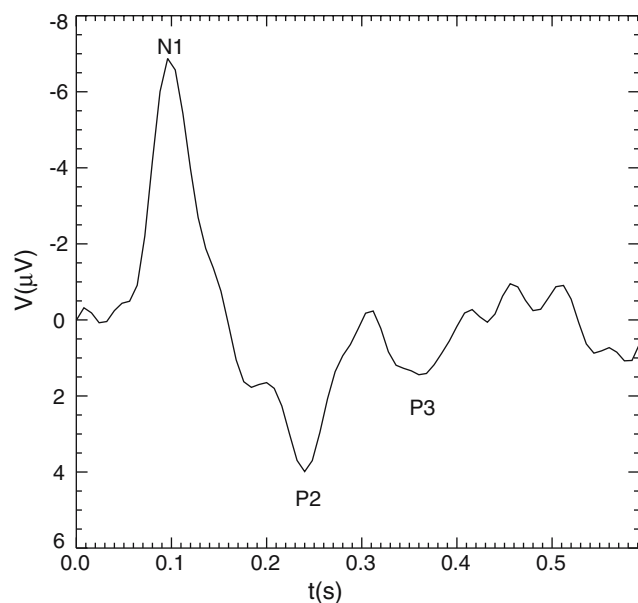
Fig. 1 Example of a CAEP for a single individual, recorded using the Cz electrode, as described in Sect. 3.1. The major features, N1, P2, and P3, are labeled

the modulation of physiological parameters in the brain that leads to these conditions results in consistent, reproducible changes in the CAEP.

Traditional methods analyze CAEPs as sequences of peaks and troughs, called "components" (Picton et al. 2000). Small, early (<20 ms) components result from brainstem nuclei; components such as N1, P2, and P3 are often attributed to early cognitive processing in the cortex; later, smaller features (>400 ms) are also attributed to the cortex, and are affected by emotional priming and other high-level processes (Schupp et al. 2006).

CAEPs are typically "scored" by listing the amplitude and latency of a predetermined set of extremums, but there are serious drawbacks to this method. Most of the information contained in the CAEP is ignored, since scoring emphasizes a handful of data points and discards the rest of the wave-form. Additionally, CAEP components are thought to result from spatiotemporal superpositions of activity from different populations of neurons (Näätänen and Picton 1987), and hence treating each component as a single, distinct phenomenon is misleading. Furthermore, since scoring is entirely phenomenological, it does not allow comparison between EEGs and CAEPs, even though they are different aspects of the same system. Although a number of disorders are marked by reliable changes in the aspects of EPs that are used in scoring (Polich and Herbst 2000), it is possible that other disorders, which are not yet known to be correlated to changes in CAEPs, could be detected using a more sophisticated method.

In addition to scoring, several other methods of CAEP analysis have been used, including equivalent dipole source

localization (e.g., Turetsky et al. 1990; Gevins 1996), wavelet analysis (Bradley and Wilson 2004), and autoregression (Mainardi et al. 2000). However, none of these methods relate CAEPs to brain physiology; even the locations of sources found using dipole modeling are not necessarily indicative of the actual locations of sources in the brain (Wood 1982; Nunez and Silberstein 2000).

To produce a more biologically relevant analysis of CAEPs based on the entire waveform, we use a physiology-based mean-field model of the brain's electrical activity to model CAEPs. Mean-field models of the brain have been used and developed over several decades (Wilson and Cowan 1973; Lopes da Silva et al. 1974; Nunez 1974, 1995; Freeman 1975; Steriade et al. 1990; Jirsa and Haken 1996; Wright and Liley 1996), and Robinson et al. developed an analytic, physiology-based continuum model, incorporating many aspects of previous models (Robinson et al. 1997, 2001b, 2002, 2005; Rennie et al. 2002; Rowe et al. 2004). Not all of the parameters in this model are known precisely from experiment (Horwitz and Glabus 2005), but all are required to lie within physiological limits, and can be estimated through inverse modeling. The predictions of this model have been verified against many types of EEG phenomena as well as independent physiological measurements (e.g., Robinson et al. 2004; Rowe et al. 2004).

In the present work, we fit a theoretical CAEP produced by the Robinson et al. model to experimental data, allowing model parameters to be deduced. This method, based on modeling the physiology underlying CAEPs rather than merely reproducing or analyzing their shape, can potentially provide more information about the subject's neurophysiological state than standard methods. Through modeling, it should be possible to use CAEPs to quantitatively estimate some of the brain's physiological parameters and their differences from resting state.

Our primary aim is to describe this method of CAEP analysis and demonstrate its potential for allowing insights not afforded by other methods. Hence, here it is applied only to data from normal subjects, with clinical applications to be discussed in future publications.

Section 2 briefly reviews the corticothalamic model of Robinson et al., including stability and sensitivity analyses. Section 3 describes the experimental subjects and methods, as well as the details of the CAEP fitting procedure. Section 4 presents the results obtained by fitting the model to experimental data, while Sect. 5 relates these results to physiology.

2 The model

This section outlines the model used in the remainder of the work. Sections 2.1–2.5 describe the neuronal, neuroanatomical, and physiological features underlying the model. Sections 2.6 and 2.7 discuss the stability of the model dynam-

ics and their sensitivity to changes in parameter values, respectively.

2.1 Overview of the model

Two key structures needed in modeling EPs resulting from simple auditory stimuli are the cortex and the thalamus. The cortex is approximated as a 2D surface (Robinson et al. 1997), and the thalamus is modeled as two functionally and anatomically distinct components: the relay nuclei and the thalamic reticular nucleus (Rennie et al. 2002).

Five distinct populations of neurons are considered: (i) cortical neurons with large characteristic ranges (denoted by the subscript e), primarily pyramidal cells, which form predominantly excitatory connections to cortical and thalamic neurons. (ii) Cortical neurons with short characteristic ranges (denoted i), including interneurons and spiny stellate cells, which form predominantly inhibitory synapses onto other cortical neurons. (iii) Thalamic sensory relay nuclei neurons (denoted s), the excitatory neurons linking the sensory modalities to the cortex. (This population also includes diffuse projection nuclei neurons, since these also provide excitatory thalamocortical connections.) (iv) Reticular thalamic neurons (denoted r), which form inhibitory connections to the main body of the thalamus, and are involved in regulating thalamic activity. (v) Sensory neurons (denoted n), which in this context are the excitatory neurons of the auditory pathway, and which transmit signals from the cochlea to the thalamus. These five populations and their interconnections are shown in Fig. 2.

Because the phenomena we are concerned with occur on scales of mm to cm, we use a continuum model of neural dynamics, which is a valid approximation for scales larger than ∼0.1 mm (e.g., Wilson and Cowan 1973; Lopes da Silva et al. 1974; Freeman 1975; Wright and Liley 1996; Robinson et al. 1997). This allows the properties of individual neurons to be replaced by the mean properties of ensembles of neurons.

The state of a given population of neurons is determined by the activity of all populations that synapse onto that population, including activity from self connections. Hence, the net effect P_a on the activity of neurons of population a by all populations of neurons b is given by

$$P_a(\mathbf{r}, t) = \sum_b v_{ab} \phi_b(\mathbf{r}, t), \tag{1}$$

where $v_{ab} \equiv N_{ab} s_b$, N_{ab} is the number of synapses from neurons of population b to population a, s_b is the strength of the postsynaptic potentials generated by neurons of population b, ϕ_b is the activity (expressed as the rate of action potentials) in neurons of population b, and the sum is over
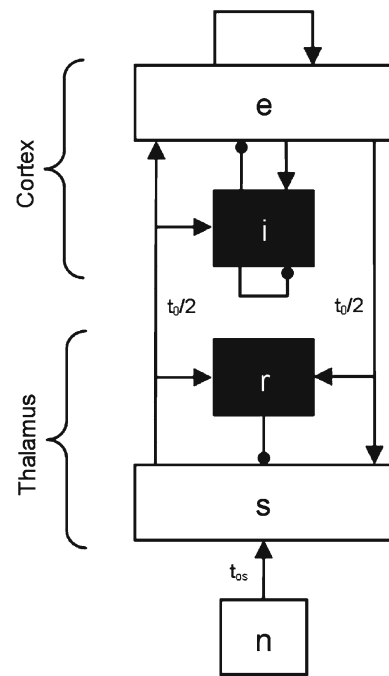

Fig. 2 The Robinson et al. corticothalamic model, consisting of the cortex (e and i), thalamic reticular nucleus (r), thalamic sensory nuclei (s), and sensory afferents (n). The excitatory and inhibitory neuron populations (*white* and *black* boxes, respectively) are interlinked by bundles of axons (*arrowheads* for excitatory connections; *circles* for inhibitory). Time delays ($t_0/2$, t_{os}) are also shown. Not all pathways are reciprocal; for example, there is no direct connection from the reticular nucleus to the cortex

all populations of neurons that have connections to neurons of population a.

2.2 Neuronal properties

The effect of synaptic activity on the postsynaptic cell's membrane potential is also affected by the passive electrical properties of dendrites and the kinetics of the neurotransmitter and its receptor, all of which attenuate high frequency components of the signal. This filtering can be approximated by the convolution kernel

$$L(t) = \frac{\alpha\beta}{\beta - \alpha} \left(e^{-\alpha t} - e^{-\beta t} \right), \tag{2}$$

for $t \geq 0$, with $L = 0$ for $t < 0$, and where $1/\beta$ and $1/\alpha$ are the rise and decay time constants, respectively. Although different populations of neurons have different values of α and β, here a single characteristic value for each is used.

The membrane potential V_a (relative to resting) for a population of neurons is approximated by a convolution of the net activity P_a and the filter function L:

$$V_a(\mathbf{r}, t) = \int_{-\infty}^{t} L(t - t') P_a(\mathbf{r}, t') dt'. \tag{3}$$
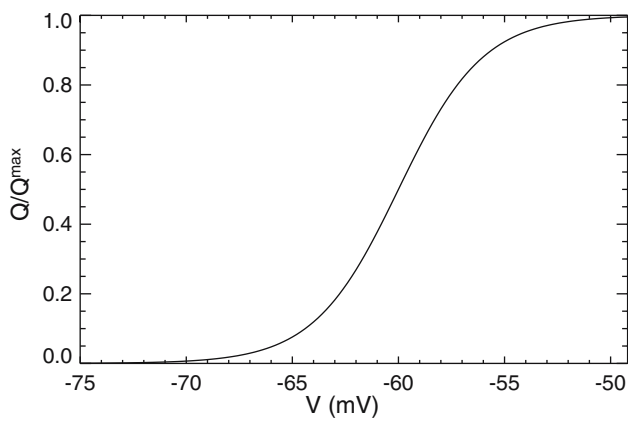
Fig. 3 The sigmoidal response function for a population of neurons, using (4) and physiological data, as a function of the membrane potential $V = V_{\text{rest}} + V_a$, where V_{rest} is the resting membrane potential and V_a is the potential relative to resting

Although the activity of a single neuron is effectively a step function of the cell body potential, a population of neurons will exhibit a sigmoidal response to increasing membrane depolarization, since cells have a distribution of threshold potentials due to variations in membrane properties. This response is approximated by

$$Q_a(\mathbf{r}, t) = \frac{Q_a^{\max}}{1 + e^{-C(V_a - \theta_a)/\sigma_a}}, \tag{4}$$

where Q_a is the firing rate, $Q_a^{\max}$ is the maximum firing rate, θ_a is the mean of the threshold distribution relative to resting, and $C = \pi/\sqrt{3}$. The derivative of (4) approximates a normal distribution, and the constant C is chosen so that the standard deviation (SD) of the derivative is equal to σ_a (Wilson and Cowan 1973; Jansen and Rit 1995; Wright and Liley 1996). This function is shown in Fig. 3.

Although (4) is nonlinear, under most conditions $\Delta V_a \lesssim \sigma_a$, and hence a linear approximation to (4) is valid (Robinson et al. 1997; Rennie et al. 1999). Thus, treating the EEG signal as being the result of small perturbations about a steady state, the response function becomes

$$Q_a(\mathbf{r}, t) \approx Q_a^{(0)} + \rho_a[V_a(\mathbf{r}, t) - V_a^{(0)}], \tag{5}$$

where

$$\rho_a \equiv \frac{dQ_a}{dV_a} = \frac{CQ_a}{\sigma_a}\left(1 - \frac{Q_a}{Q_a^{\max}}\right) \tag{6}$$

is evaluated at steady state. It is not necessary to determine the steady state firing rate $Q_a^{(0)}$, as only perturbations to this value are used in the model. Using (6), we can relate these perturbations in the activity from neurons of population b to perturbations in the activity of neurons of population a by defining linear gains G_{ab}:

$$G_{ab} = \frac{\Delta Q_a}{\Delta Q_b} = \rho_a N_{ab} s_b . \tag{7}$$

The net gain of more than two populations of neurons connected serially is simply the product of the separate gains, and such compound gains are written as $G_{ab}G_{bc} = G_{abc}$, for example.

Finally, to relate the neuronal activity ϕ_a to the average membrane potential Q_a, we use a damped wave equation to approximate the propagation of neuronal activity in the cortex (Nunez 1995; Jirsa and Haken 1996; Robinson et al. 1997; Rennie et al. 1999, 2002). Hence,

$$D_a\phi_a(\mathbf{r}, t) = Q_a(\mathbf{r}, t) , \tag{8}$$
$$D_a = \frac{1}{\gamma_a^2}\left[\frac{\partial^2}{\partial t^2} + 2\gamma_a\frac{\partial}{\partial t} + \gamma_a^2 - v_a^2\nabla^2\right], \tag{9}$$

where $\gamma_a = v_a/r_a$ is the damping rate, v_a is the axonal propagation velocity, and r_a is the characteristic range of axons for neurons of population a. Since cortical inhibitory neurons have short ($\sim 10^{-4}$ m) axonal processes, we assume $r_i \approx 0$, and hence $D_i \approx 1$ (Robinson et al. 1997); the same approximation can be made for intrathalamic connections, and thus $D_s \approx D_r \approx 1$.

2.3 Transfer functions

Since the scalp potential measured using EEG techniques is directly related to ϕ_e (Nunez 1995; Nunez and Srinivasan 2006), and since the stimulus is defined as being ϕ_n, determining the scalp potential from the stimulus requires the transfer function ϕ_e/ϕ_n. To obtain this transfer function, we first Fourier transform (1)–(5), (8), and (9), allowing the evaluation of perturbations to the steady state. Assuming that a signal traveling from the thalamus to cortex takes a time $t_0/2 = r_{ct}/v_{ct}$, where v_{ct} is the thalamocortical propagation velocity and r_{ct} is the distance from the thalamus to the cortex, we find that (1) becomes

$$P_e(\mathbf{k}, \omega) = v_{ee}\phi_e + v_{ei}\phi_i + v_{es}\phi_s \, e^{i\omega t_0/2}, \tag{10}$$
$$P_i(\mathbf{k}, \omega) = v_{ie}\phi_e + v_{ii}\phi_i + v_{is}\phi_s \, e^{i\omega t_0/2}, \tag{11}$$
$$P_s(\mathbf{k}, \omega) = v_{se}\phi_e e^{i\omega t_0/2} + v_{sr}\phi_r + v_{sn}\phi_n, \tag{12}$$
$$P_r(\mathbf{k}, \omega) = v_{re}\phi_e e^{i\omega t_0/2} + v_{rs}\phi_s, \tag{13}$$

where $\mathbf{k}$ is the wavenumber and ω is the frequency. Equations (2), (3), (4), and (9) become

$$L(\omega) = (1 - i\omega/\alpha)^{-1} (1 - i\omega/\beta)^{-1}, \tag{14}$$
$$V_a(\mathbf{k}, \omega) = L(\omega)P_a(\mathbf{k}, \omega), \tag{15}$$
$$Q_a(\mathbf{k}, \omega) = \rho_a V_a(\mathbf{k}, \omega), \tag{16}$$
$$D_a(\mathbf{k}, \omega)\phi_a(\mathbf{k}, \omega) = Q_a(\mathbf{k}, \omega), \tag{17}$$
$$D_e(\mathbf{k}, \omega) = k^2 r_e^2 + (1 - i\omega/\gamma)^2, \tag{18}$$
$$D_i = D_s = D_r = 1 . \tag{19}$$

The transfer function ϕ_e/ϕ_n is found by eliminating P, V, and Q from (10) to (19). Assuming random cortical connectivity (i.e., $G_{ab} = G_{cb}$ for all combinations where a, b, c are either e or i; Wright and Liley 1996), the component of this transfer function for an impulse traveling directly from the thalamus to the cortex is given by

$$\mathcal{I} = \frac{e^{i\omega t_0/2} L^2 G_{esn}}{1 - L^2 G_{srs}}, \tag{20}$$

the modulation of this signal by cortical feedback is

$$\mathcal{M}_c = D_e(1 - LG_{ei}) - LG_{ee}, \tag{21}$$

and the modulation by corticothalamic loops is

$$\mathcal{M}_t = \frac{e^{i\omega t_0}(L^2 G_{ese} + L^3 G_{esre})}{1 - L^2 G_{srs}}. \tag{22}$$

The transfer function is given by combining (20)–(22), which yields

$$T(\mathbf{k}, \omega) \equiv \frac{\phi_e(\mathbf{k}, \omega)}{\phi_n(\mathbf{k}, \omega)} = \frac{\mathcal{I}}{\mathcal{M}_c - \mathcal{M}_t}. \tag{23}$$

2.4 Stimulus

We can approximate the incoming stimulus arising from the sensory neurons as a Gaussian in both space and time. Such a stimulus has the normalized form

$$\phi_n(\mathbf{r}, t) = \frac{e^{-\frac{1}{2}\left(\frac{t - t_{os}}{t_s}\right)^2}}{t_s\sqrt{2\pi}} \frac{e^{-\left(\frac{|\mathbf{r} - \mathbf{r}_{os}|}{r_s}\right)^2}}{\pi r_s^2}, \tag{24}$$

where t_s is the characteristic duration of the stimulus, t_{os} is the transmission delay from cochlea to thalamus, r_s is the spatial width of the stimulus at cortex, and $\mathbf{r}_{os}$ is the offset of the center of the stimulus from the point of measurement. The Fourier transform of this function is

$$\phi_n(\mathbf{k}, \omega) = e^{-\frac{1}{2}\omega^2 t_s^2} e^{i\omega t_{os}} e^{-\left(\frac{k r_s}{2}\right)^2} e^{-i\mathbf{k}\cdot\mathbf{r}_{os}}. \tag{25}$$

The stimulus parameters t_s, t_{os}, r_s and $\mathbf{r}_{os}$ should be considered effective values, as the actual spatiotemporal structure of the impulse is likely to be much more complex than that modeled here. However, one advantage of using a spatially Gaussian stimulus is that it implicitly incorporates the effects of volume conduction, which can be approximated for low to moderate wavenumbers by a filter function of the form (Srinivasan et al. 1998; Robinson et al. 2001b; O'Connor et al. 2002)

$$F(k) = e^{-k^2/k_0^2}, \tag{26}$$

where $F(k)$ is the square of the ratio of scalp to cortical voltages and $k_0 \approx 30\,\mathrm{m}^{-1}$.

2.5 Evoked potential

To evaluate the response of the cortical neurons ϕ_e to the stimulus, we must inverse Fourier transform the product of (23) and (25):

$$R(\mathbf{r}, t) = \frac{1}{(2\pi)^3} \iint \frac{\phi_e(\mathbf{k}, \omega)}{\phi_n(\mathbf{k}, \omega)} \phi_n e^{i\mathbf{k}\cdot\mathbf{r}} e^{-i\omega t} d\omega\, d^2\mathbf{k}. \tag{27}$$

Considering first the spatial inverse Fourier transform, we find

$$R(\mathbf{r}, \omega) = \frac{1}{(2\pi)^2} \int \frac{\phi_e(\mathbf{k}, \omega)}{\phi_n(\mathbf{k}, \omega)} e^{-\left(\frac{k r_s}{2}\right)^2} e^{-i\mathbf{k}\cdot\mathbf{r}_{os}} e^{i\mathbf{k}\cdot\mathbf{r}} d^2\mathbf{k}, \tag{28}$$

$$= \frac{1}{(2\pi)^2} \int_0^\infty k \frac{\phi_e(\mathbf{k}, \omega)}{\phi_n(\mathbf{k}, \omega)} e^{-\left(\frac{k r_s}{2}\right)^2} \int_0^{2\pi} e^{ik|\mathbf{r} - \mathbf{r}_{os}|\cos\theta} d\theta dk, \tag{29}$$

$$= \frac{1}{2\pi} \int_0^\infty k \frac{\phi_e(\mathbf{k}, \omega)}{\phi_n(\mathbf{k}, \omega)} e^{-\left(\frac{k r_s}{2}\right)^2} J_0(k|\mathbf{r} - \mathbf{r}_{os}|)\, dk, \tag{30}$$

where J_0 is a Bessel function of the first kind.

In the case where $r_s \to 0$ (i.e., the stimulus is spatially delta-like), (30) has an analytic solution, given by

$$\frac{1}{2\pi} \int_0^\infty k \frac{\phi_e(\mathbf{k}, \omega)}{\phi_n(\mathbf{k}, \omega)} J_0(k|\mathbf{r} - \mathbf{r}_{os}|)\, dk = \frac{\mathcal{I} K_0(q|\mathbf{r} - \mathbf{r}_{os}|)}{2\pi r_e^2(1 - LG_{ei})}, \tag{31}$$

where $\mathcal{I}$ is defined by (20), K_0 is a modified Bessel function of the second kind, and

$$q = \frac{1}{r_e}\sqrt{\left(1 - \frac{i\omega}{\gamma}\right)^2 - \frac{LG_{ee} + \mathcal{M}_t}{1 - LG_{ei}}}. \tag{32}$$

As an alternative to using infinite boundary conditions, one can define characteristic circumferences of the cortex l_x and l_y (representing the cortical dimensions in the coronal and frontal planes, respectively) and sum over discrete wavenumbers corresponding to the modes of the system. Assuming a rectangular cortex with periodic boundary conditions, $R(\mathbf{r}, \omega)$ can be evaluated using

$$R(\mathbf{r}, \omega) = \frac{1}{l_x l_y} \sum_{m,n=-\infty}^{\infty} \frac{\phi_e(\mathbf{k}_{mn}, \omega)}{\phi_n(\mathbf{k}_{mn}, \omega)} e^{-\left(\frac{k r_s}{2}\right)^2} e^{i\mathbf{k}_{mn}\cdot(\mathbf{r} - \mathbf{r}_{os})}, \tag{33}$$
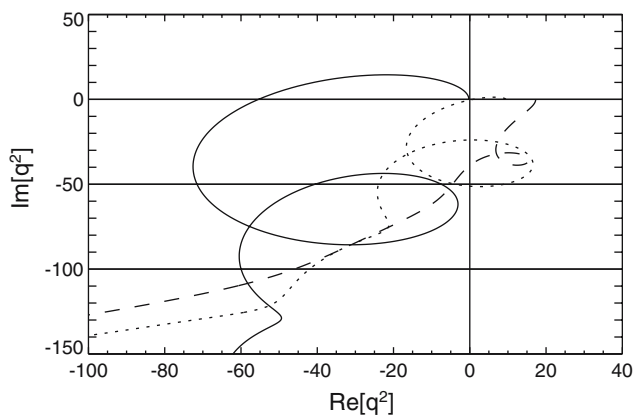
Fig. 4 Three plots of q^2. These show stable (*dashed*), marginally stable (*dotted*), and unstable (*solid*) states. The initial point of each locus lies on the real axis and other points correspond to $\omega > 0$

where

$$\mathbf{k}_{mn} = \left(\frac{2\pi m}{l_x}, \frac{2\pi n}{l_y} \right), \tag{34}$$

and $k = |\mathbf{k}_{mn}|$. Typically, the sum (33) produces almost identical results to the integral case (30), except very near to certain resonances, or in the physiologically unrealistic case $l_x, l_y \lesssim r_e$ (Robinson et al. 2001a).

Finally, to obtain the CAEP waveform $R(\mathbf{r}, t)$, we perform an inverse Fourier transform in the time domain, and multiply by a normalization factor N that incorporates the unknown amplitudes of (i) the stimulus, (ii) the gain G_{esn} between the auditory neurons and the cortex, and (iii) the ratio of scalp to cortical voltages:

$$R(\mathbf{r}, t) = \frac{N}{2\pi} \int R(\mathbf{r}, \omega) e^{-\frac{1}{2}(\omega t_s)^2} e^{i\omega t_{os}} e^{-i\omega t} d\omega. \tag{35}$$

This equation, together with (23) and (33), yields a CAEP time series based on the input parameters.

2.6 Model stability

The stability condition for the model is that Re $q > 0$ (32), which is equivalent to the condition that q^2 is never simultaneously negative and real (Robinson et al. 1997, Robinson et al. 2001b). If this condition does not hold, the transfer function becomes unbounded for some combination of ω and $\mathbf{k}$, which corresponds to the amplitude of oscillations increasing rather than decreasing exponentially with time. Three examples of q^2 at various levels of stability are shown in Fig. 4.

The stability of the brain is primarily a function of the balance between excitation and inhibition, and we can parameterize this balance using three stability parameters.

The cortical stability parameter X is

$$X = \frac{G_{ee}}{1 - G_{ei}}, \tag{36}$$

the corticothalamic stability parameter Y is

$$Y = \frac{G_{ese} + G_{esre}}{(1 - G_{ei})(1 - G_{srs})}, \tag{37}$$

and the intrathalamic stability parameter Z is

$$Z = -G_{srs} \frac{\alpha\beta}{(\alpha + \beta)^2}. \tag{38}$$

Together X, Y, and Z define a three-dimensional space, within which a region of stability exists (Robinson et al. 2002). If the parameters lie outside this region, instability results, with the frequency of the instability depending on which of the instability boundaries is crossed.

A special case of the requirement Re $q > 0$ is that $q^2 > 0$ when $\omega = 0$ (Robinson et al. 2002). The value of $q^2 r_e^2$ at this point is denoted S; from (32) we see

$$S = 1 - X - Y. \tag{39}$$

If $S < 0$, the transfer function is unbounded at zero frequency for some wavenumber, and the system is unstable.
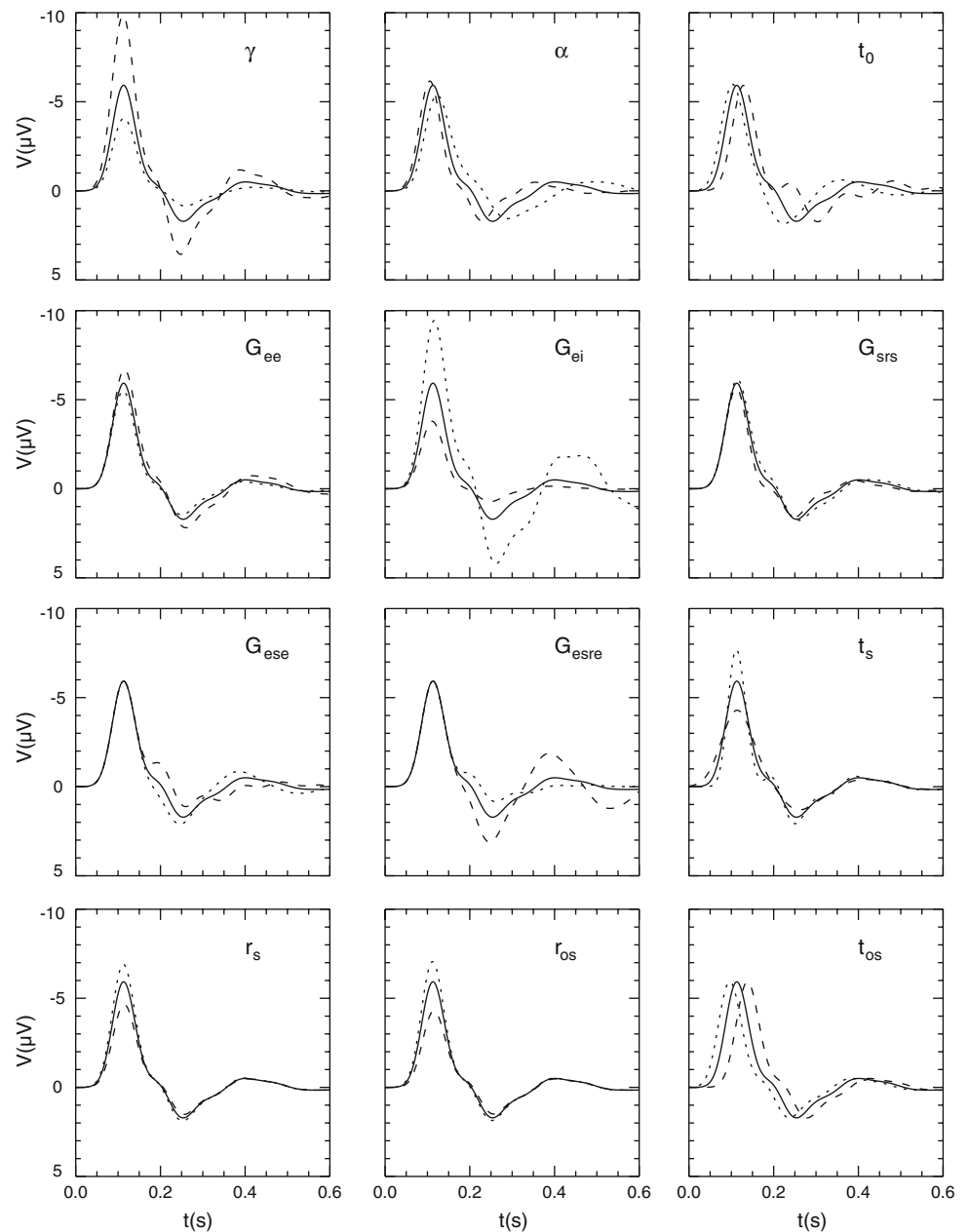
2.7 Parameter sensitivities

The model is significantly more sensitive to some parameters than others; the parameters to which the model is sensitive are shown in Fig. 5, and the qualitative effects of varying each parameter are described below. While we use a linearized approximation to the model (5), with the exception of the overall scaling factor N, all parameters have a nonlinear effect on the shape of the curve.

Small changes in the cortical damping rate γ and the decay rate α affect the amplitude and latency of peaks, respectively, while large changes in either affect all aspects of the CAEP. Changes in the rise rate β have little effect; since rise times are typically about one tenth of decay times (Koch et al. 1996), we fix $\beta = 10\alpha$ in the remainder of this work.

Increasing the intracortical excitatory gain G_{ee} tends to increase the magnitude of the CAEP, as expected, with the greatest effect being on N1. Increasing the magnitude of the cortical inhibitory gain G_{ei} uniformly reduces the amplitude of all CAEP features. Decreasing $|G_{ei}|$ may lead to slow-wave instability, as seen in Fig. 5.

The $\sim$10 Hz oscillation associated with increasing the corticothalamic excitatory loop G_{ese} is related to the alpha rhythm in EEGs. Similarly, increasing the corticothalamic inhibitory loop $|G_{esre}|$ accentuates the $\sim$4 Hz theta rhythm,

Fig. 5 Sensitivity of the theoretical CAEP to variation of model parameters, as labeled in the corner of each frame. The *solid line* is the CAEP corresponding to the nominal parameter values (Table 1); the *dotted line* indicates a 50% decrease in magnitude of a given parameter, while a *dashed line* indicates a 50% increase

with the frequencies of these oscillations determined by the time delay in each loop. The gains G_{ese} and G_{esre} have opposing effects, as shown in Fig. 5, where the curve corresponding to increased G_{ese} is similar to the curve corresponding to decreased $|G_{esre}|$. Increasing $|G_{esre}|$ with respect to G_{ese} causes Y to become negative, which leads to a shift in the dominant frequency from ∼10 Hz (alpha band) to ∼4 Hz (theta band). Increases in the magnitude of the intrathalamic inhibitory loop G_{srs} cause oscillations with sleep spindle frequency (∼15 Hz), which is expected since the reticular nucleus plays a major role in their generation (Steriade et al. 1993).

One of the most important parameters of the model is the corticothalamic delay t_0, as modulations of t_0 change the temporal position of the CAEP features. Even a small change in t_0 has clear effects on the CAEP, since it changes the relative phases of the components of the waveform generated by the corticothalamic pathways, leading to constructive and destructive interference.

Increasing the stimulus duration t_s produces temporal low-pass filtering of the CAEP; changing the temporal stimulus offset t_{os} shifts the CAEP in time but does not change its shape. The effects of the spatial stimulus width r_s and offset r_{os} are more complicated, depending on both their relative

and absolute values. In general, increasing either quantity decreases the magnitude of the response, and also produces temporal low-pass filtering due to the relationship between spatial and temporal frequencies given by the dispersion relation (18). While this filtering is not as obvious as it is for t_s, the N1 feature has a larger high-frequency component than the P2 feature, and hence low-pass filtering will tend to decrease the amplitude of N1 as compared to P2, as seen in Fig. 5.

3 Experimental methods

This section discusses the application of the model outlined in Sect. 2 to experimental data. Section 3.1 details the acquisition of the EEG data, Sect. 3.2 describes the process by which the model was used to determine brain parameters from this data, and Sect. 3.3 clarifies the assumptions made in the fitting procedure.

3.1 Data acquisition

The two sets of data from normal subjects were obtained from the Brain Resource Company (BRC) International Database (Gordon et al. 2005), from which subjects were excluded if they had been exposed to factors (disease, injury, etc.) that are known to affect performance in psychometric tests. The first dataset contained parameter values from fits to eyes-open EEG data and the second contained CAEP data. Subjects from both datasets were evenly distributed in age from 21 to 56 years.

Recordings were made at 26 sites of the international 10–20 system using an electrode cap, following previously published methods for acquisition and artifact removal (Rowe et al. 2004; Gordon et al. 2005). EEG data were recorded at a 125 Hz sampling rate and an A/D precision of 0.42 µV through a SynAmps™ amplifier using a linked earlobe reference and a low-pass third-order Butterworth filter with a –6 dB point at 50 Hz. Eye movements were corrected offline using the method of Gratton et al. (1983). Only data from the Cz electrode are reported here, as this electrode receives less noise from muscle artifacts than other electrodes and records the most prominent N1 and P2 components (Key et al. 2005).

In the first experimental condition, eyes-open EEG data were recorded for three minutes from 313 subjects (165 females, 148 males). Spectral fitting to this data was done by the BRC using the method given by Rowe et al. (2004).

In the second experimental condition, CAEP data were recorded from 214 subjects (108 females, 106 males). Subjects were presented binaurally, via headphones, with a series of high and low tones, at 75 dB and lasting for 50 ms, with a constant interstimulus interval (ISI) of 1 s. Rise and fall times of the tones were 5 ms. Subjects were instructed to press buttons with the index finger of each hand in response
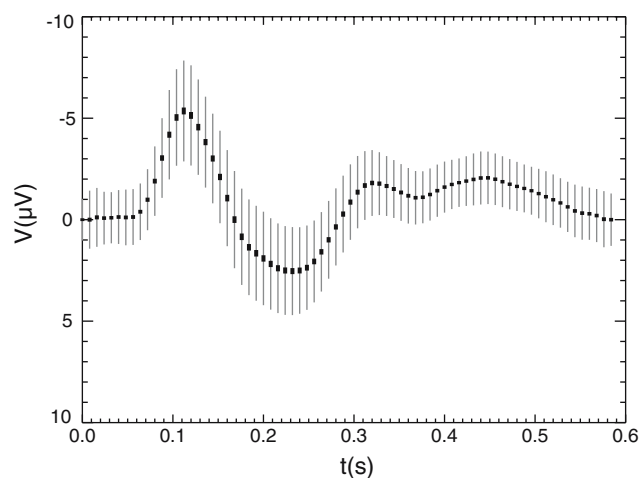

Fig. 6 Grand mean standard CAEP from 214 normal subjects. Standard deviation is shown by the *vertical lines*, and SEM is shown by the heights of the *rectangles*

to "target" tones (presented at 1,000 Hz). They were asked not to respond to "standard" tones (presented at 500 Hz). Subjects were given a brief practice session to clarify the distinction between target and standard stimuli. Speed and accuracy of response were stressed equally in the task instructions. There were 280 standard and 60 target tones presented in a quasi-random order, with the only constraint being that two targets could not appear consecutively. Subjects were told that the duration of the auditory oddball task was six minutes. Mean standard CAEPs were obtained by averaging the 280 periods following standard stimuli. A grand mean standard CAEP was produced by averaging the mean CAEPs over all subjects; this CAEP is shown in Fig. 6.

3.2 CAEP fitting procedure

In addition to the experimental CAEP data to be fitted, a set of nominal values of model parameters is required to produce a theoretical CAEP to initialize the fitting. The choice of nominal parameter values is based on the null hypothesis that there are no differences between resting EEG and standard CAEP states. While this hypothesis was rejected, as shown in Fig. 7, it provides the reference point from which parameters can be subsequently varied. However, EEG fitting does not provide any estimates of the stimulus parameters, so initial values of these parameters were obtained by identifying physiologically plausible ranges for each and by finding the values within those ranges for which the theoretical curve has peak width and latency characteristics most similar to CAEP data.

After an initial theoretical CAEP is generated, the χ^2 value (goodness of fit) between the experimental and theoretical CAEPs is calculated using
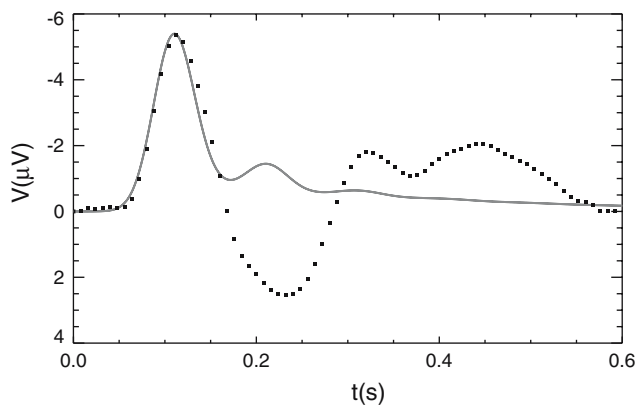
Fig. 7 Comparison of the theoretical CAEP produced by nominal eyes-open EEG parameters (*solid line*) and standard CAEP data (*squares*). Parameter values are as given in Table 1. The poor correspondence between the theoretical and experimental CAEPs shows that brain parameters differ between resting EEG and CAEP states

$$\chi^2 = \sum_{i=0}^{n-1} \left(\frac{D(i) - T(i)}{W(i)} \right)^2 , \qquad (40)$$

where n is the number of points in the time series, D is the experimental CAEP time series, T is the theoretical time series, and W is a weight function. The weight function is such that data points are weighted by a factor of 1 from 0–300 ms, 0.5 from 300–400 ms, and 0.25 from 400–600 ms, thus assigning greater significance to the earlier features of the waveform, as later features are likely dependent upon cortical interactions beyond the scope of our current model (Goodin et al. 1978).

Fitting is performed by varying the parameters of the theoretical CAEP to minimize χ^2 using the Levenberg-Marquardt method of χ^2 minimization (Press et al. 1992). In this stage of fitting, parameters are allowed to vary without bound. Ideally, the parameters would converge to the global minimum χ^2 from anywhere within a large region of parameter space, and hence the choice of initial parameter values would be unimportant to the final result of the fit. However, this is not necessarily the case, as there may be multiple minimums in χ^2 for each parameter, as shown in Fig. 8.

The task of finding the global minimum value of χ^2 is further complicated by the high dimensionality of parameter space. To overcome these difficulties, a Monte Carlo method is used to vary the initialization of each parameter. The distribution of parameter values used for the initializations is a Gaussian with a mean equal to the nominal value and an SD of 40% of the mean; after these initializations, the fitting routine is run with the new initial parameters. This process is repeated thousands of times to obtain a statistical distribution, from which the fits that successfully found the global minimum χ^2 are determined.
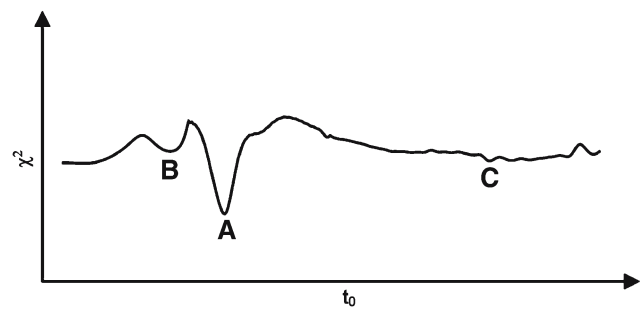

Fig. 8 Schematic diagram of goodness-of-fit (χ^2) as a function of the corticothalamic loop delay t_0, showing several qualitative features of parameter space. Prior to the application of the fit selection criteria, randomly initialized trials converge on both the global minimum (*A*) and on local minimums (e.g., *B*). Small, local features (e.g., *C*) may be circumvented in other dimensions of parameter space

Once the fits to EEG and CAEP data have been calculated, a subset of these fits is selected using four criteria. First, fits are excluded if their χ^2 value is above a certain threshold, as this indicates that the fit did not find the global minimum. Second, fits are rejected if they violate any of the stability criteria defined in Sect. 2.6. Third, fits are rejected if any parameters are unphysical (e.g., a negative time delay) or have values outside the physiologically accepted limits. We find that only about 30% of trials are actually eliminated as a result of this criterion; the remainder fall naturally within the physiological limits. The fact that the fit parameters converge on physiologically reasonable values even in the absence of constraints is one of the key aspects of the model, and is discussed further in Sect. 4. Finally, remaining fits are excluded if at least one parameter is more than two SDs from the mean. This eliminates fits that found χ^2 minimums in distant parts of parameter space, and hence are not in the main basin of attraction. These fits are eliminated because they are typically extremely sensitive to small perturbations in parameter values, and it is impossible to reach these regions of parameter space without crossing instabilities.

The result of applying these selection criteria is that the parameter distributions are unimodal and approximately Gaussian, which allows each distribution to be characterized by its mean value and SD. The parameters of these remaining trials are averaged to obtain an estimated value and uncertainty for each parameter.

3.3 Implicit assumptions

The fitting approach requires four primary assumptions. First, it is assumed that the function $\chi^2(\mathbf{p})$, where $\mathbf{p}$ is the vector of parameters, has a global minimum clearly distinguishable from local minimums. If no clear global minimum exists for a given parameter, the uncertainty in the value of that parame-

ter is determined by the range over which the local minimums are distributed.

Second, it is assumed that the limits chosen for the parameters are physiologically reasonable. All parameters are consistent with known limits; however, the true ranges of many parameters are not accurately known, and the ranges which are ultimately allowed are likely to be narrower than current estimates.

Third, it is assumed in our calculations that parameter values are constant throughout the CAEP. While stimulus-induced changes will necessarily be transient, it is assumed that these changes can be approximated to sufficient accuracy by using a single parameter value. This assumption becomes increasingly tenuous with time, and likely explains why early features are modeled better than later ones, as discussed in Sect. 4. The use of constant parameter values also assumes that the sources of the CAEP remain fixed; this approximation is made because our aim is to explain the data using as simple a model as possible, with further elaborations added only when required.

Finally, it is assumed that the grand mean CAEP accurately represents the effects of robust physical processes. This is similar to the assumption, made in almost all research on EPs, than the mean EP obtained by averaging over hundreds of stimuli in a given subject adequately reflects the essential processes occurring in the brain.

4 Experimental results

After the selection criteria described in Sect. 3.2 were applied, the remaining fits were all good matches to data, especially for the N1 and P2 features, as shown in Fig. 9. To our knowledge, these results are the closest fits to CAEPs to date using physiological modeling (cf. Rennie et al. 2002; David et al. 2006). The naïve view that we have used a dozen independent parameters to fit two features of a CAEP is incorrect, since (i) many parameters have similar effects, (ii) parameter variations are restricted by stability and physiological considerations, and (iii) the model is limited in the types of responses it can produce; it cannot fit arbitrary curves. Additionally, there is no a priori reason why the model should produce CAEPs at all, as it was not designed for this purpose. Furthermore, parameter values which generate CAEPs are close to values obtained from EEG fitting, as expected, and lie within physiological limits. This agreement with physiology was found for approximately 70% of fits even without externally-imposed constraints, providing independent evidence that the model parameters successfully characterize the physiology of the system.

The vast majority of the contribution to χ^2 in our fits comes from the second half of the CAEP time window ($t > 300$ ms); for a typical fit, only 2% of the contribution
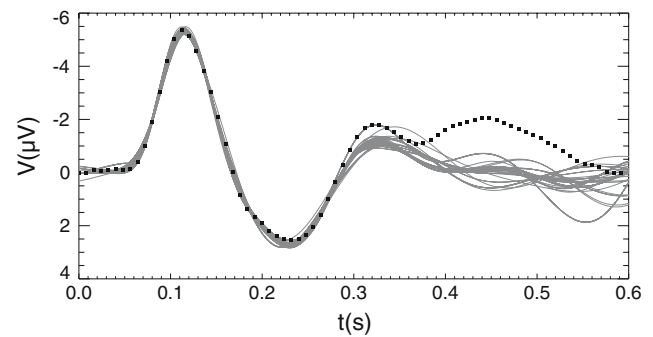

Fig. 9 Comparison between experimental CAEP data (*squares*) and a randomly selected subset of 40 theoretical trial fits which remained after the fit selection criteria were applied (*solid lines*)

comes from the first half. This is likely caused by three factors. First, we use constant parameter values for the duration of the CAEP, and the validity of this approximation decreases with time. Second, late features are associated with memory, emotion, and other high-level cognitive aspects (Schupp et al. 2006), which may depend upon brain regions that are not considered separately in our current corticothalamic model, but are instead grouped with other regions. Although future models will incorporate such complexity as required, our aim here is to reproduce the major features of the CAEP as simply as possible.

Uncertainties in parameter values obtained through modeling are difficult to determine precisely, since these are determined by the region of parameter space that produces acceptable fits. The size of this region can be estimated qualitatively by determining the consistency of the fitted parameter values following perturbations to (i) the nominal parameter values, (ii) the fit selection criteria, and (iii) the experimental data. These perturbations do not usually have significant effects on the results, implying that this region of parameter space has reasonably well-defined boundaries. It was found empirically that the SDs of the parameter distributions give uncertainty estimates which are in good agreement with the qualitative tests listed above. Hence, although not statistically exact, these SDs can be taken as quantitative estimates of the uncertainty in parameter values. Estimates of parameter values and their SDs are summarized in Table 1.

4.1 Gains

All gains except the intrathalamic gain G_{srs} showed notable differences between resting EEG and CAEP fits. Both cortical and corticothalamic excitatory gains (G_{ee} and G_{ese}, respectively) had decreased magnitude in CAEP fits compared to resting EEG fits, while cortical and corticothalamic inhibitory gains (G_{ei} and G_{esre}, respectively) had increased magnitude, collectively producing a shift from excitation to inhibition. The most consistent differences were in the

Table 1 Parameter values and standard deviations for resting eyes-open EEG and standard CAEPs. Values which differ by more than one SD between EEG and CAEP fits are marked with asterisks

Parameter	Symbol	EEG ($\pm$SD)	CAEP ($\pm$ SD)	Unit
Cortical damping rate	γ*	67 ± 30	200 ± 30	s^{-1}
Dendritic decay rate	α*	96 ± 37	45 ± 2	s^{-1}
Corticothalamic loop delay	t_0*	84 ± 14	64 ± 4	ms
Cortical excitatory gain	G_{ee}	5.6 ± 3.8	3.1 ± 1.6	–
Cortical inhibitory gain	G_{ei}	-6.9 ± 3.9	-10.8 ± 1.7	–
Corticothalamic excitatory gain	G_{ese}*	7.7 ± 5.0	0.8 ± 0.7	–
Corticothalamic inhibitory gain	G_{esre}	-5.3 ± 4.2	-7.8 ± 2.1	–
Intrathalamic gain	G_{srs}	-0.8 ± 0.5	-0.8 ± 0.1	–
Cortical stability	X*	0.7 ± 0.2	0.3 ± 0.1	–
Corticothalamic stability	Y*	0.2 ± 0.2	-0.3 ± 0.1	–
Intrathalamic stability	Z	0.1 ± 0.1	0.1 ± 0.01	–
Zero frequency stability	S*	0.1 ± 0.1	1.1 ± 0.2	–
Temporal stimulus offset	t_{os}	–	50 ± 4	ms
Temporal stimulus width	t_s	–	23 ± 1	ms
Spatial stimulus offset	r_{os}	–	0.14 ± 0.03	m
Spatial stimulus width	r_s	–	0.09 ± 0.09	m

corticothalamic gains G_{ese} and G_{esre}, although these gains also had the broadest distributions.

In our model, the excitatory corticothalamic gain G_{ese} enhances activity in the alpha band (8–12 Hz), while the inhibitory corticothalamic gain G_{esre} enhances activity in the theta band ($\sim$4 Hz). While EEG spectra show a strong peak in the alpha band, such a peak is lacking in CAEPs, which are dominated by activity in the theta band; hence, we would expect a decrease in G_{ese} and an increase in the magnitude of G_{esre}, as observed.

A simple picture of the preceding results emerges if we consider the stability parameters X, Y, Z, and S, introduced in Sect. 2.6. Most notably, Y reverses sign, indicating that the corticothalamic loop changes from producing positive to negative feedback; the decrease in X indicates that the ratio of excitation to inhibition in the cortex also decreases. These changes correspond to increased stability, and this is dramatically shown by the change in S—for parameters obtained from fits to resting EEG spectra, S is close to the instability boundary ($S \approx 0$; Robinson et al. 2005), while for fits to CAEPs, the system is extremely stable ($S > 1$). These changes are shown in Fig. 10.

4.2 Temporal parameters

Changes in the cortical damping rate γ and the dendritic rate constant α, though large, were not highly reproducible. This is because increases in γ can be partially offset by decreases in α, resulting in multiple minimums during fitting.

To investigate this interaction, CAEP fits were repeated with α fixed at its nominal EEG value. As expected, γ values
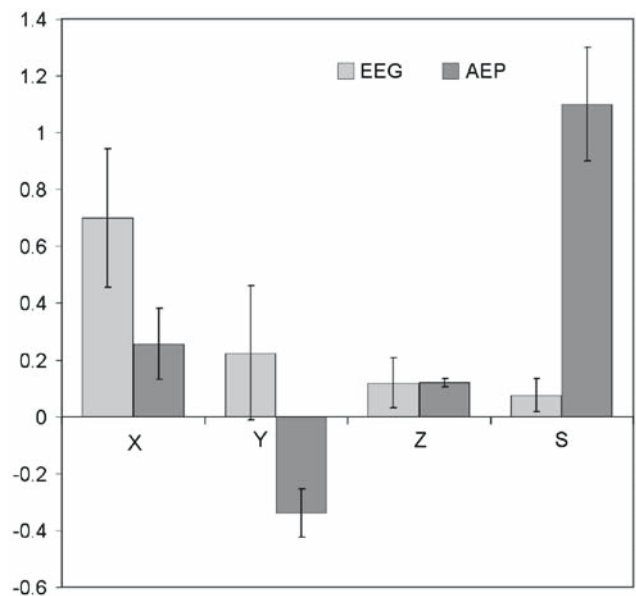

Fig. 10 Differences in stability parameters X, Y, Z, and S between EEG and CAEP states. Note the sign change in Y, indicating inhibitory thalamocortical feedback, and the increase in S, indicating greater stability. *Error bars* show standard deviations

obtained from these fits (140 ± 35 s^{-1}) were closer to those found from EEG fits; the values of other parameters were not notably different from fits where α was allowed to vary.

Although small, the difference in the corticothalamic delay t_0 between resting EEG and CAEPs is robust, as it is highly constrained by the alpha peak frequency of the EEG (Rowe et al. 2004) and by the latencies of CAEP components.

4.3 Stimulus parameters

In contrast to other model parameters, the stimulus parameters are not comparable to EEG, since the stimulus used in resting EEG fits was spatiotemporal white noise (Robinson et al. 1997).

Both temporal stimulus parameters are strongly constrained by the N1 feature of the CAEP. The latency of this feature is given by $t = t_{os} + t_0/2$, where t_{os} is the temporal stimulus offset. Since t_0 is robust, it follows that the stimulus offset t_{os} can be accurately determined. Similarly, the width of the N1 feature is determined predominantly by the stimulus duration t_s. As a result, both of these parameters have narrow distributions.

The spatial stimulus offset (r_{os}) and width (r_s) are more poorly constrained, as their primary effect is to reduce high spatiotemporal frequencies that are already damped given typical values of t_s. Both parameters lie within physiological ranges, however. Interestingly, $r_s = 0.09$ m is equivalent to a volume conduction parameter k_0 (see Sect. 2.4) of $22\,\text{m}^{-1}$, which agrees very well with previous estimates (O'Connor et al. 2002), implying that r_s is dominated by volume conduction effects.

5 Discussion

We have shown that by fitting our physiology-based model to experimental CAEP data, self-consistent and reproducible estimates of model parameters can be obtained. In this section, we suggest some possible physiological interpretations of these results.

The key advantage of physiology-based modeling is that the fitted model parameters give us information about brain physiology that is only accessible by invasive means, if at all. The changes in parameters found using this model accord with such invasive experiments done on other animals: the increases in cortical and thalamic inhibition found here are consistent with microelectrode and depth electrode recordings in rats (Meeren et al. 2001; Barth and Di 1990), suggesting that the CAEP generation mechanisms in rats are similar to those implied by our model in humans.

One of the complications of both experimentation and modeling is the considerable complexity of even a single feature of the CAEP—Näätänen and Picton (1987) found seven separate sources of the auditory N1 feature, many of which are fairly localized. The process of averaging used to produce EPs effectively selects these active networks, while filtering out activity from other regions in the brain. Hence, the parameters reported here likely do not reflect changes in the whole brain, but instead describe the state of networks specific to CAEP generation. For example, the observed increase in inhibition could be explained by increased excitation in a focal area of cortex, surrounded by a large area of increased inhibition. Such lateral inhibition is a widespread phenomenon in the nervous system (Blakemore et al. 1970; Houtgast 1972; Margrie et al. 2001), and several authors have postulated that it is the basis of focal attention (Crick 1984; Sokolov et al. 2002).

The possibility of specific networks being selected in the CAEP also invites a possible explanation for the decrease in the corticothalamic delay t_0. This change implies an increase in the corticothalamic conduction velocity, which suggests that networks with greater conduction velocities are recruited (or weighted more heavily) in stimulus processing. This is consistent with neuroanatomical studies showing that axons from the relay nuclei of the thalamus are more myelinated than those of the diffuse thalamocortical projection system (Salami et al. 2003). Additionally, our estimate of t_0 is similar to the empirically determined time delay required for attention switching (Crick 1984; McDonald et al. 2005), consistent with the hypothesis that the thalamus is essential to stimulus processing.

As with conventional theories of information processing in the brain (Ashwin and Timme 2005), our model predicts that the brain operates near an instability boundary (Robinson et al. 2002). However, in order to respond to stimuli efficiently, the networks that process these stimuli must respond transiently ($< 1\,$s). In our model, this implies a high degree of damping, and hence a high level of stability within these networks. As expected, the parameters corresponding to CAEPs are further from instability than the parameters for resting EEG.

The values of the gains observed here are strikingly similar to those reported for sleep states (Robinson et al. 2002). Although there are obvious behavioral differences between sleep and CAEPs, it is notable that both are dominated by theta activity. While it cannot be concluded that the same pathway is involved, it does appear that the pathways used in both sleep and CAEPs have similar latencies, which would be expected if both are the result of corticothalamic negative feedback loops. Additionally, several studies have shown increased amplitudes of certain CAEP components, particularly P2, during sleep (Nordby et al. 1996; Nielsen-Bohlman et al. 1991). These findings were most pronounced in slow-wave sleep, while CAEPs elicited during REM sleep resemble those during waking. These studies suggest that the mechanism by which delta activity is enhanced in sleep may also enhance certain CAEP components.

Another similarity between slow-wave sleep and CAEPs is a reduction in the dendritic rate constant α compared to resting EEG (Robinson et al. 2004). Since α is a weighted average of multiple rate constants, this difference could be produced by changes in the relative activity of AMPA/kainate and GABA$_\text{A}$ neurons (for which $\alpha \approx 50$–$200\,\text{s}^{-1}$; Hausser and Roth 1997; Otis and Mody 1992) to NMDA and GABA$_\text{B}$

neurons (for which $\alpha \approx 5\text{–}10\,s^{-1}$; Spruston et al. 1995; Otis et al. 1993). Even a small recruitment of NMDA and GABA$_B$ neurons could reduce the effective decay rate significantly.

6 Conclusion

We have developed a physiology-based method of analyzing EPs based on a quantitative corticothalamic mean-field model. This model produced excellent fits to experimental CAEP data, and the parameters of the fits were used to suggest the physiological basis of CAEP generation. These parameters converged to physiologically realistic values even in the absence of external constraints, providing strong support for the validity of the model. Furthermore, the observed differences in parameter values between resting EEG and CAEP states agree with previous studies on CAEP generation, and provide insights into possible similarities between CAEPs and other brain phenomena.

The advantages of this method of EP analysis compared to standard methods are significant, including: (i) it is objective and automated; (ii) it is based on physiology, and the fitted parameters provide quantitative information on underlying brain physiology; (iii) EEG and EP data are treated in a unified manner; (iv) the entire EP waveform is used, in contrast to standard techniques which typically use only the amplitudes and latencies of a few predetermined features; and (v) our method may allow features to be distinguished which are too subtle to be detected using other methods.

The application of this method to experimental data has shown that CAEPs can be generated by changes in the gains of corticothalamic loops, due to either modulations of an existing network, or to the recruitment of additional networks with different parameter values. This agrees with the well-established view that corticothalamic pathways are essential to stimulus processing and hence CAEP generation. Additionally, similarities between CAEPs and slow-wave sleep were observed, with both phenomena appearing to be generated by corticothalamic negative feedback loops. Future applications of our method of EP analysis include quantitative investigations of the physiology of aging and disease.

References

Ashwin P, Timme M (2005) Nonlinear dynamics: when instability makes sense. Nature 436:36–37

Barth DS, Di S (1990) Three-dimensional analysis of auditory-evoked potentials in rat neocortex. J Neurophysiol 64:1527–1536

Blakemore C, Carpenter RH, Georgeson MA (1970) Lateral inhibition between orientation detectors in the human visual system. Nature 228:37–39

Bradley AP, Wilson WJ (2004) On wavelet analysis of auditory evoked potentials. Clin Neurophysiol 115:1114–1128

Crick F (1984) Function of the thalamic reticular complex: the searchlight hypothesis. Proc Natl Acad Sci USA 81:4586–4590

David O, Kiebel SJ, Harrison LM, Mattout J, Kilner JM, Friston KJ (2006) Dynamic causal modeling of evoked responses in EEG and MEG. Neuroimage 30:1255–1272

Freeman W (1975) Mass action in the nervous system. Academic Press, New York

Gevins A (1996) High resolution evoked potentials of cognition. Brain Topogr 8:189–199

Goodin DS, Squires KC, Starr A (1978) Long latency event-related components of the auditory evoked potential in dementia. Brain 101:635–648

Gordon E, Cooper N, Rennie C, Hermens D, Williams LM (2005) Integrative neuroscience: the role of a standardized database. Clin EEG Neurosci 36:64–75

Gratton G, Coles M, Donchin E (1983) A new method for off-line removal of ocular artifact. Electroencephalogr Clin Neurophysiol 55:468–484

Hausser M, Roth A (1997) Estimating the time course of the excitatory synaptic conductance in neocortical pyramidal cells using a novel voltage jump method. J Neurosci 17:7606–7625

Horwitz B, Glabus MF (2005) Neural modeling and functional brain imaging: the interplay between the data-fitting and simulation approaches. Int Rev Neurobiol 66:267–290

Houtgast T (1972) Psychophysical evidence for lateral inhibition in hearing. J Acoust Soc Am 51:1885–1894

Jansen BH, Rit VG (1995) Electroencephalogram and visual evoked potential generation in a mathematical model of coupled cortical columns. Biol Cybern 73:357–366

Jirsa VK, Haken H (1996) Field theory of electromagnetic brain activity. Phys Rev Lett 77:960–963

Key AP, Dove GO, Maguire MJ (2005) Linking brainwaves to the brain: an ERP primer. Dev Neuropsychol 27:183–215

Koch C, Rapp M, Segev I (1996) A brief history of time (constants). Cereb Cortex 6:93–101

Kotchoubey B (2005) Event-related potential measures of consciousness: two equations with three unknowns. Prog Brain Res 150:427–444

Lopes da Silva FH, Hoeks A, Smits H, Zetterberg LH (1974) Model of brain rhythmic activity. The alpha rhythm of the thalamus. Kybernetik 15:27–37

Mainardi LT, Kupila J, Nieminen K, Korhonen I, Bianchi AM, Pattini L, Takala J, Karhu J, Cerutti S (2000) Single sweep analysis of event related auditory potentials for the monitoring of sedation in cardiac surgery patients. Comput Methods Programs Biomed 63:219–227

Margrie TW, Sakmann B, Urban NN (2001) Action potential propagation in mitral cell lateral dendrites is decremental and controls recurrent and lateral inhibition in the mammalian olfactory bulb. Proc Natl Acad Sci USA 98:319–324

McDonald JJ, Teder-Salejarvi WA, Di Russo F, Hillyard SA (2005) Neural basis of auditory-induced shifts in visual time-order perception. Nature Neurosci 8:1197–1202

Meeren HK, van Cappellen van Walsum AM, van Luijtelaar EL, Coenen AM (2001) Auditory evoked potentials from auditory cortex, medial geniculate nucleus, and inferior colliculus during sleep-wake states and spike-wave discharges in the WAG/Rij rat. Brain Res 898:321–331

Näätänen R, Picton T (1987) The N1 wave of the human electric and magnetic response to sound: a review and an analysis of the component structure. Psychophysiology 24:375–425

Nielsen-Bohlman L, Knight RT, Woods DL, Woodward K (1991) Differential auditory processing continues during sleep. Electroencephalogr Clin Neurophysiol 79:281–290

Nordby H, Hugdahl K, Stickgold R, Bronnick KS, Hobson JA (1996) Event-related potentials (ERPs) to deviant auditory stimuli during sleep and waking. Brain Res Rev 7:1082–1086

Nunez PL (1974) Wave-like properties of the alpha rhythm. IEEE Trans Biomed Eng 21:473–482

Nunez PL (1995) Neocortical dynamics and human EEG rhythms. Oxford University Press, New York

Nunez PL, Silberstein RB (2000) On the relationship of synaptic activity to macroscopic measurements: does co-registration of EEG with fMRI make sense? Brain Topogr 13:79–96

Nunez PL, Srinivasan R (2006) A theoretical basis for standing and traveling brain waves measured with human EEG with implications for an integrated consciousness. Clin Neurophysiol 117:2424–2435

O'Connor SC, Robinson PA, Chiang AKI (2002) Wave-number spectrum of electroencephalographic signals. Phys Rev E 66:061905

Otis TS, Mody I (1992) Modulation of decay kinetics and frequency of GABAA receptor-mediated spontaneous inhibitory postsynaptic currents in hippocampal neurons. Neuroscience 49:13–32

Otis TS, De Koninck Y, Mody I (1993) Characterization of synaptically elicited GABAB responses using patch-clamp recordings in rat hippocampal slices. J Physiol 463:391–407

Picton TW, Bentin S, Berg P, Donchin E, Hillyard SA, Johnson R, Miller GA, Ritter W, Ruchkin DS, Rugg MD, Taylor MJ (2000) Guidelines for using human event-related potentials to study cognition: recording standards and publication criteria. Psychophysiology 37:127–152

Polich J, Herbst K (2000) P300 as a clinical assay: rationale, evaluation, and findings. Int J Psychophysiol 38:3–19

Press WH, Flannery BP, Teukolsky SA, Vetterling WT (1992) Numerical Recipes in C. Cambridge University Press, Cambridge

Rennie CJ, Robinson PA, Wright JJ (1999) Effects of local feedback on dispersion of electrical waves in the cerebral cortex. Phys Rev E 59:3320–3329

Rennie CJ, Robinson PA, Wright JJ (2002) Unified neurophysical model of EEG spectra and evoked potentials. Biol Cybern 86:457–471

Robinson PA, Rennie CJ, Wright JJ (1997) Propagation and stability of waves of electrical activity in the cerebral cortex. Phys Rev E 56:826–840

Robinson PA, Loxley PN, O'Connor SC, Rennie CJ (2001) Modal analysis of corticothalamic dynamics, electroencephalographic spectra, and evoked potentials. Phys Rev E 63:041909

Robinson PA, Rennie CJ, Wright JJ, Bahramali H, Gordon E, Rowe DL (2001) Prediction of EEG spectra from neurophysiology. Phys Rev E 63:021903

Robinson PA, Rennie CJ, Rowe DL (2002) Dynamics of large-scale brain activity in normal arousal states and epileptic seizures. Phys Rev E 65:041924

Robinson PA, Rennie CJ, Rowe DL, O'Connor SC (2004) Estimation of multiscale neurophysiologic parameters by electroencephalographic means. Hum Brain Mapp 23:53–72

Robinson PA, Rennie CJ, Rowe DL, Connor SC, Gordon E (2005) Multiscale brain modeling. Phil Trans R Soc B 360:1043–1050

Rowe DL, Robinson PA, Rennie CJ (2004) Estimation of neurophysiological parameters from the waking EEG using a biophysical model of brain dynamics. J Theor Biol 231:413–433

Salami M, Itami C, Tsumoto T, Kimura F (2003) Change of conduction velocity by regional myelination yields constant latency irrespective of distance between thalamus and cortex. Proc Nat Acad Sci USA 100:6174–6179

Schupp HT, Flaisch T, Stockburger J, Junghofer M (2006) Emotion and attention: event-related brain potential studies. Prog Brain Res 156:31–51

Sokolov EN, Nezlina NI, Polyanskii VB, Evtikhin DV (2002) The orientating reflex: the 'targeting reaction' and 'searchlight of attention'. Neurosci Behav Physiol 32:421–437

Spruston N, Jonas P, Sakmann B (1995) Dendritic glutamate receptor channels in rat hippocampal CA3 and CA1 pyramidal neurons. J Physiol 482:325–352

Srinivasan R, Nunez PL, Silberstein RB (1998) Spatial filtering and neocortical dynamics: Estimates of EEG coherence. IEEE Trans Biomed Eng B 45:814–826

Steriade M, Gloor P, Llinás RR, Lopesda Silva FH, Mesulam MM (1990) Basic mechanisms of cerebral rhythmic activities. Electroencephalogr Clin Neurophysiol 76:481–508

Steriade M, McCormick DA, Sejnowski TJ (1993) Thalamocortical oscillations in the sleeping and aroused brain. Science 262:679–685

Turetsky B, Raz J, Fein G (1990) Representation of multi-channel evoked potential data using a dipole component model of intracranial generators: application to the auditory P300. Electroencephalogr Clin Neurophysiol 76:540–556

Wilson HR, Cowan JD (1973) A mathematical theory of the functional dynamics of cortical and thalamic nervous tissue. Kybernetik 13:55–80

Wood CC (1982) Application of dipole localization methods to source identification of human evoked potentials. Ann N Y Acad Sci 388:139–155

Wright JJ, Liley DTJ (1996) Dynamics of the brain at global and microscopic scales: neural networks and the EEG. Behav Brain Sci 19:285–294